Wet-Chemical Synthesis of Doped Nanoparticles: Optical Properties of Oxygen-Deficient and Antimony-Doped Colloidal SnO$_2$

Tanjew Nütz and Markus Haase*

Institut für Physikalische Chemie, Universität Hamburg, Bundesstrasse 45, D-20146 Hamburg, Germany

Received: May 25, 2000; In Final Form: June 19, 2000

Blue-colored aqueous colloids of n-doped tin dioxide nanoparticles in the 4−9-nm size regime have been prepared hydrothermally either by inducing oxygen vacancies into the SnO$_2$ lattice or by doping the nanoparticles with antimony. Autoclavation at temperatures above 250 °C is found to be necessary to achieve n-doping of the particles. Blue-colored oxygen-deficient nanoparticles are obtained in the absence of antimony by employing a reducing atmosphere inside the autoclave. If these colloids are exposed to air, their blue color vanishes within 1 day, indicating back reaction of the vacancies with oxygen. Antimony-doped tin dioxide nanoparticles have been prepared by using either Sb^{III}Cl$_3$ or Sb^{V}Cl$_5$ as the source of antimony. In contrast to the oxygen-deficient tin dioxide, the blue color of antimony-doped nanoparticles is stable in air. The blue color of the colloids corresponds to a broad absorption peak in the red and IR regions, independent of the method of n-doping. As for bulk material, this IR absorption is interpreted as a plasma excitation of free carriers in the n-doped nanoparticles. High-resolution TEM images and X-ray powder diffraction patterns confirm the high crystallinity of the nanoparticles and the same rutile lattice structure as known from bulk SnO$_2$.

Introduction

Bulk tin dioxide that is either nonstoichiometric or doped with atoms such as fluorine or antimony shows a high n-type conductivity.[1] At high enough doping levels, a degenerate semiconductor is obtained, displaying metallic properties such as a very weak dependence of the electrical conductivity on temperature.[2−4] These observations are in accord with quantum mechanical calculations of the electronic structure of highly doped SnO$_2$:Sb, showing that the antimony ions lead to a partially filled free-electron-like impurity band in the band gap of tin dioxide.[5]

Because of the presence of free carriers in the crystal lattice, crystals and conductive films of SnO$_2$:Sb exhibit a high absorption coefficient in the NIR and IR regions, rendering them highly reflective for IR radiation.[6,7] The IR spectrum can be well described[4] by applying simple Drude theory for a free-electron gas.[8,9] According to Drude theory, the absorption onset, the shape, and the intensity of the IR absorption are mainly determined by the number density of free electrons and the mean time between two electron scattering events. In the case of bulk material, the IR absorption appears as a broad band with a steplike shape. For separated spherical metal nanoparticles, however, a different absorption spectrum is obtained. In this case, according to Mie theory, the plasma absorption of the bulk metal is compressed into a narrow peak (plasmon polariton). The latter has been well investigated for metal nanoparticles such as silver and gold.[10,11]

The free carrier concentration in SnO$_2$:Sb can be varied easily by changing the concentration of dopant atoms. If the content of dopant is high, the absorption onset is located in the red, and the material shows a bluish color. At lower dopant concentrations, the absorption onset is situated in the NIR, i.e., the material is transparent throughout the visible region. The number density of free electrons and the mean time between two electron scattering events also determine the electrical conductivity of the single-crystalline domains in the sample. Values for these two quantities can be obtained by fitting the IR spectrum to Drude theory.[4] For bulk samples, for which the electrical conductivity is not dominated by grain boundary effects, the measured conductivity agrees well with the conductivity calculated from these values.

Layers of SnO$_2$:Sb have found widespread interest[12] because of their potential applications in photovoltaic and optoelectronic devices, flat panel displays, etc. These films can be prepared, for instance, by spray-coating or dip-coating glass substrates with a solution containing appropriate tin and antimony precursors or with colloidal tin dioxide containing antimony. However, n-conductivity is only observed when the deposited films are annealed at typically 500 °C or when the precursor solution is sprayed directly onto a heated substrate. Thus, incorporation of the dopant into the host lattice takes place in the dry state and at elevated temperatures.

The results presented here are part of a series of papers dealing with the properties of colloids of n-doped SnO$_2$ nanoparticles and porous layers of such particles. Electrically conductive antimony-doped tin dioxide nanocrystals can be prepared in aqueous solution if the synthesis is performed at elevated temperatures in an autoclave.[13,14] Inside an autoclave, the liquid-phase synthesis can be performed in water, although temperatures of more than about 250 °C[13] are required to yield colloidal solutions of deeply blue-colored SnO$_2$:Sb nanocrystals. As-deposited layers of these nanoparticles exhibit rather strong grain-boundary resistance,[13,14] and the IR absorption spectrum consists of a broad peak,[13] which can be described by Mie theory. To change the shape of the IR absorption spectrum from a peak to a step, the latter being expected for a bulk metal, the nanoparticle layer must be sintered at temperatures as high as 900 °C.[13] These results indicate isolated or only weakly interacting nanoparticles in as-deposited layers. Thus, nanopar-

Wet-Chemical Synthesis of Doped Nanoparticles

J. Phys. Chem. B, Vol. 104, No. 35, 2000 **8431**

ticle layers of SnO$_2$:Sb prepared at lower temperatures still exhibit many properties of isolated particles. The optical and spectroelectrochemical properties of nanoporous SnO$_2$:Sb layers have been discussed in recent publications by Boschloo and Fitzmaurice[15] and by us.[16] The results again indicate a thin layer of insulating material around each nanoparticle as the reason for the large grain-boundary resistance of the layers and for their peak-shaped absorption spectrum.

In a further investigation,[17] we used X-ray absorption spectroscopy to determine the oxidation state and the local environment of antimony in powders of nanocrystalline SnO$_2$: Sb after treatment at different temperatures. The experiments indicate a SnO$_2$ environment of antimony even if the material is heated to 100 °C only. If an antimony(III) source is used in the synthesis, incorporation of antimony into the tin dioxide lattice is accompanied by rapid oxidation to antimony(V), which, in contrast to the large antimony(III) ion, has a smaller ionic radius than tin(IV). Furthermore, the results indicate that the formation of the n-conductive phase proceeds in two steps: In the first step, a nonconductive mixed oxide of tin and antimony with a slightly distorted rutile structure is formed. During the second step, which takes place upon heating of the nanocrystalline powder to 500 °C in air, the oxygen content of this mixed oxide changes toward the composition Sn$_{1-x}$Sb$_x$O$_2$ of the n-conductive phase.

Investigation of this second step is complicated by the two different oxidation states of antimony (III and V) and by the presence of water and hydroxyl groups at the particle surface impeding reliable measurements of the oxygen content of the crystal lattice.

In this paper, we use an autoclave to study the conversion of the colloidal mixed oxide to the n-conductive phase in more detail. Inside an autoclave, oxidizing or reducing conditions can be easily adjusted by selecting an appropriate atmosphere. We show how the oxidation state of the antimony precursor, the duration of heating, and the atmosphere inside the autoclave affect the changes in optical absorption that accompany the formation of the n-conductive phase. Moreover, we demonstrate that blue-colored colloids of tin dioxide are not only obtained by doping with antimony, but also by introducing oxygen vacancies into the lattice. All of the absorption spectra presented here are measured on colloidal solutions, i.e., on samples in which the particles are well separated from each other.

Experimental Section

Preparation of Colloidal Solutions. Colloidal solutions of tin dioxide and tin antimony oxide were prepared according to literature procedures[18−20] and converted into blue-colored colloids of n-doped tin dioxide nanoparticles by autoclavation at 270 °C, as described previously.[13] Tin dioxide nanoparticles doped with 6 atom % of antimony were prepared by using either SbCl$_3$ or SbCl$_5$ as the source of antimony.

In brief, 85 mmol of SnCl$_4$ were dissolved in fuming HCl (37 wt %). In the case of antimony-doped colloids, 5.43 mmol of SbCl$_3$ or SbCl$_5$ were added. The clear solution was dropped into 500 mL of water at 0 °C and cooled in an ice bath. After the mixture was stirred for 30 min, aqueous ammonia (25%) was added dropwise until a pH value of 3−4 was reached. The white precipitate obtained was allowed to settle overnight. The precipitate was washed twice with water and subsequently stirred overnight in about 300 mL of water containing 1 vol % of aqueous ammonia (25%). A turbid colloidal solution was obtained, which was dialyzed (dialysis tubing, Serva, 14146)

against 10 L of aqueous ammonia of pH 9.5−10. The resulting transparent colloidal solution was diluted to 500 mL and finally refluxed at 100 °C for 4 h. After being refluxed, antimony-doped colloids exhibited a brownish color if Sb^{III}Cl$_3$ had been employed. In the absence of antimony or if Sb^{V}Cl$_5$ had been used as the antimony source, colorless colloids were obtained.

Aliquots of 50−100 mL of these colloids were poured into glass vessels and heated to 270 °C for up to 4 days in a water bath inside an autoclave. Autoclavation in the absence of oxygen was performed by purging the autoclave with argon prior to heating. In experiments for which a reducing atmosphere was desired, a weighed amount of magnesium turnings was added to the water bath inside the autoclave before purging with argon. Hence, at elevated temperatures, hydrogen was generated by the reaction between water and magnesium, resulting in a reducing atmosphere of Ar and H$_2$ in an 1:1 ratio. After autoclavation, the colloidal solutions of SnO$_2$ or SnO$_2$:Sb nanocrystals were stored in capped glass vessels.

The antimony content of the SnO$_2$:Sb-particles was checked using both inductively coupled plasma atomic emission spectroscopy (ICP-AES) and flame atomic absorption spectroscopy (F-AAS). Colloids prepared with nominal amounts of 6.0 atom % of Sb^{III}Cl$_3$ and 6.0 atom % of Sb^{V}Cl$_5$ contained 6.2 ± 0.4 and 5.5 ± 0.4 atom % of antimony, respectively. Hence, the antimony used in the synthesis has been completely incorporated into the colloidal particles.

Powders. Powders of nanocrystalline tin dioxide were prepared by removing the solvent of the respective colloidal solution with a rotary evaporator (bath temperature of 50 °C).

Characterization Techniques. The UV−vis−NIR absorption of SnO$_2$ and SnO$_2$:Sb nanocrystals was measured by placing the aqueous colloids in quartz cuvettes with a thickness of 1 mm or 0.1 mm and recording the absorption spectra with a Cary 500 UV−vis−NIR spectrophotometer. All spectra were measured against water as the reference. The strong NIR absorption bands of water restrict the wavelength range in which the absorption of the nanoparticles can be measured. The use of 1-mm cuvettes (Suprasil, Hellma) allowed absorption measurements up to 1850 nm, whereas the use of 0.1-mm cuvettes (Infrasil, Starna) extended the usable wavelength range to 2450 nm.

High-resolution electron micrographs of the particles were recorded using a Philips CM 300 UT transmission electron microscope (TEM), operating at an acceleration voltage of 300 kV. The microscope was equipped with a CCD camera (Gatan, model 694).

X-ray powder diffraction patterns of nanocrystalline powders were acquired with a Philips Xpert XRD system, using Cu K_α radiation.

Results and Discussion

Figure 1 shows the powder X-ray diffraction patterns of tin dioxide nanocrystals prepared by three different methods. Parts a−c of the figure show the XRD data of doped colloids prepared with SbCl$_5$ as the antimony source, doped colloids in which SbCl$_3$ was used instead of SbCl$_5$, and colloids prepared in the absence of antimony, respectively. Autoclavation was carried out in air for 3 h. In all three cases, the peak positions agree well with the reflections of bulk SnO$_2$ (cassiterite, part d), indicating the same rutile lattice structure. No other crystalline phase was observed in any of the X-ray diffraction patterns. The broadening of the peaks indicates a small crystalline domain size. This can be roughly quantified using the Debye−Scherrer
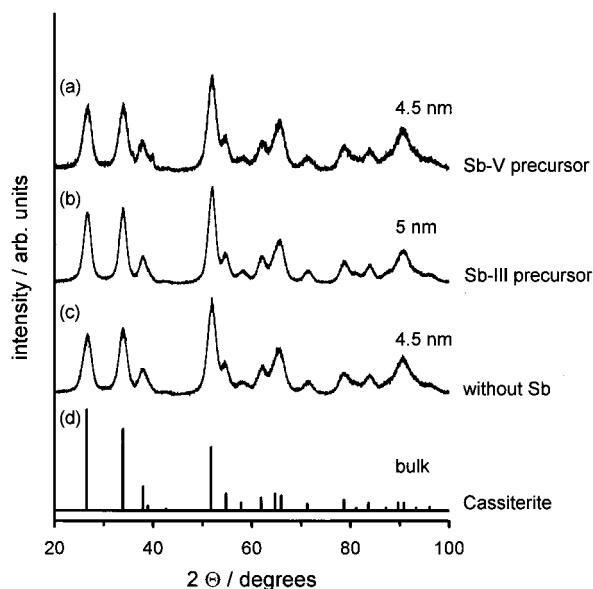
Figure 1. X-ray powder diffraction patterns of SnO_2 and SnO_2:Sb powders. (a−c) Colloids prepared using $SnCl_4$ and the indicated Sb precursor after autoclavation in air for 3 h at 270 °C; (d) highly crystalline SnO_2 (cassiterite).

formula for spherical particles, resulting in the domain sizes indicated on the figure.

These mean domain sizes are in accord with the particle size distributions observed in high-resolution TEM images of the corresponding SnO_2:Sb colloids (Figure 2). The micrographs show a large fraction of particles ranging from about 4 to 6 nm in size and a small fraction of larger particles with a diameter up to 9 nm. Lattice fringes are observed for most particles, indicating their high crystallinity. The particles are of spherical to ellipsoidal shape and tend to form string-like agglomerates. Similar images are obtained for all colloids investigated.

Figure 3 shows the UV−vis−NIR spectra of aqueous colloidal solutions of pure tin dioxide after being heated at 270 °C under different atmospheres in an autoclave. Tin dioxide colloids heated in air or under argon show no absorption except for the strong valence-to-conduction band transition in the UV. In contrast, colloids heated under a reducing atmosphere, i.e., under a 1:1 mixture of Ar and H_2, develop a blue color. The latter is caused by a broad additional absorption in the IR, which extends to the red. As already mentioned in the Experimental Section, the absorption spectra of the aqueous colloids are measured against water as the reference. The slight distortion in the spectra at about 1450 nm is caused by a strong absorption band of water, shown in the inset of the figure.

The blue color of tin dioxide nanoparticles prepared under reducing conditions is not stable if the colloid is exposed to oxygen. When the colloidal solution is stirred in air, the absorption in the near-infrared (NIR) region vanishes completely within 24 h (Figure 4). The IR absorption can be explained by the formation of oxygen vacancies in the crystal lattice, produced upon heating of the nanoparticles in a reducing atmosphere. In fact, bulk tin dioxide is well known to form oxygen vacancies easily when heated under reducing conditions.[12] The oxygen vacancies form electron-donor states located about 140 meV below the conduction band.[21−24] Consequently, oxygen-deficient bulk tin dioxide exhibits n-type conductivity at room temperature. The presence of free carriers is the reason for a considerable IR absorption of the material. Formation of oxygen-deficient n-conductive tin dioxide can be described by the
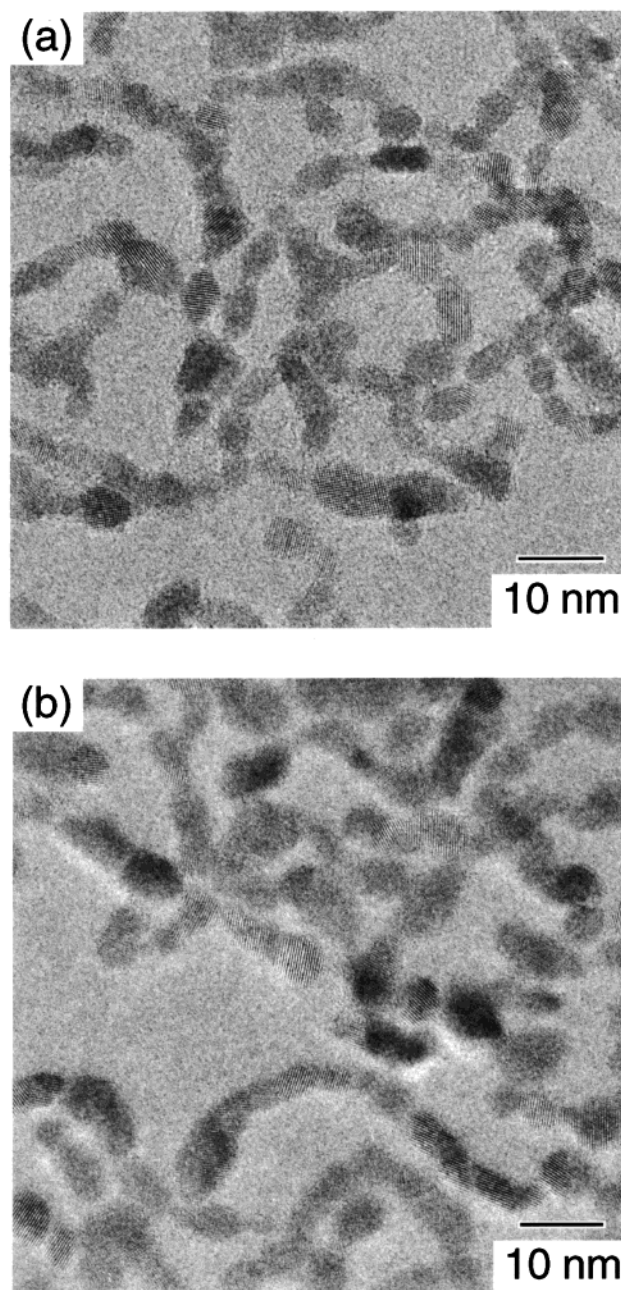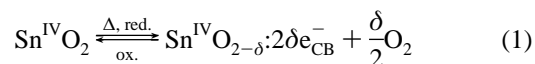

Figure 2. High-resolution TEM pictures of SnO_2:Sb colloids after autoclavation in air for 3 h at 270 °C. The preparation was carried out using (a) $SbCl_5$ and (b) $SbCl_3$ as the source of antimony.

reaction scheme

$$Sn^{IV}O_2 \underset{\text{ox.}}{\overset{\Delta, \text{red.}}{\rightleftharpoons}} Sn^{IV}O_{2-\delta}:2\delta e_{CB}^- + \frac{\delta}{2}O_2 \qquad (1)$$

The back reaction to stoichiometric tin dioxide is included in the reaction scheme, because films of polycrystalline tin dioxide with high concentrations of oxygen vacancies are known to exhibit a decrease in conductivity upon prolonged exposure to air.[25] The spectra shown in Figures 3 and 4 indicate that a similar reaction takes place in our colloidal tin dioxide nanocrystals. This back reaction with oxygen to stoichiometric tin dioxide proceeds much faster in the colloidal systems, as the surface-to-volume ratio of the nanoparticles is considerably higher and the distance between the surface and the center of the particle is small.
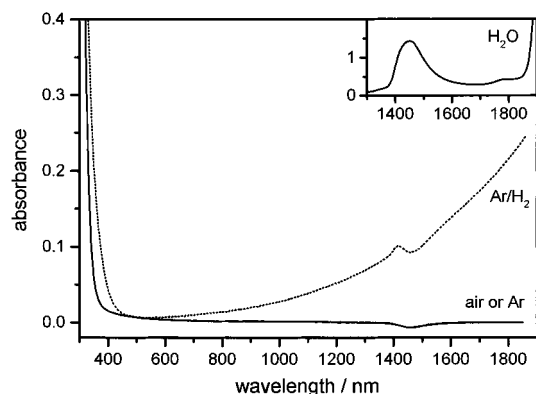
Wet-Chemical Synthesis of Doped Nanoparticles

J. Phys. Chem. B, Vol. 104, No. 35, 2000 **8433**

Figure 3. UV−vis−NIR absorption spectra of SnO_2 colloids after autoclavation for 3 h at 270 °C under the indicated atmospheric conditions. Inset: NIR absorption spectrum of the water reference. The spectra have been acquired in 1-mm cuvettes.
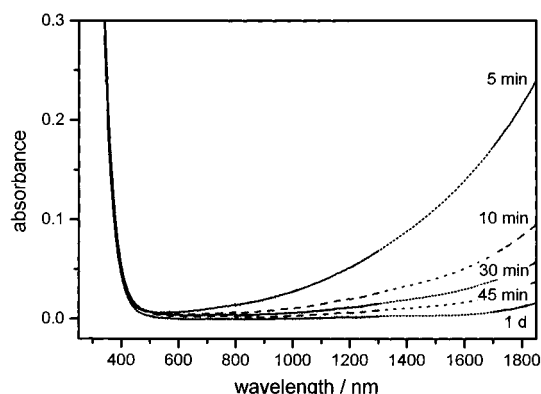

Figure 4. UV−vis−NIR absorption spectra of a SnO_2 colloid after autoclavation for 3 h at 270 °C under Ar/H_2 and subsequent exposure to air for the indicated periods of time. The spectra have been acquired in 1-mm cuvettes.

For technical applications, layers of either fluorine-doped or antimony-doped tin dioxide are used, which show stable electrical conductivity.[12] Antimony ions brought into the crystal lattice of bulk tin dioxide are known to substitute for tin ions and exhibit the oxidation state of +5. The dopant ions form electron-donor states in the material, similar to oxygen vacancies. At low antimony concentrations, the energy of the donor states has been determined to be about 35 meV below the conduction band,[23] resulting in n-type conductivity at room temperature.

If tin dioxide nanoparticles are prepared in the presence of an Sb(V) source, a colorless transparent colloid is obtained, which remains colorless even after being refluxed at 100 °C. If the colloid is heated at 270 °C for 3 h, however, it develops a strong blue color, which is caused again by a broad, structureless absorption in the red and IR regions (Figure 5). In contrast to oxygen-deficient tin dioxide nanoparticles (Figures 3 and 4), the color already develops upon heating in air or under an argon atmosphere. As for antimony-doped bulk material, the color of these colloids is stable in air. Using the requirements of charge neutrality and balanced masses, conversion of the colorless nonconductive mixed antimony tin oxide, $(1 − x)SnO_2 \cdot (x/2)$-Sb_2O_5 to n-conductive antimony-doped tin dioxide can be written as

$$(1 − x)\,SnO_2 \cdot \frac{x}{2}Sb_2^{V}O_5 \xrightarrow{\Delta} (Sn_{1−x}Sb_x^{V})O_2 : xe_{CB}^{-} + \frac{x}{4}O_2$$
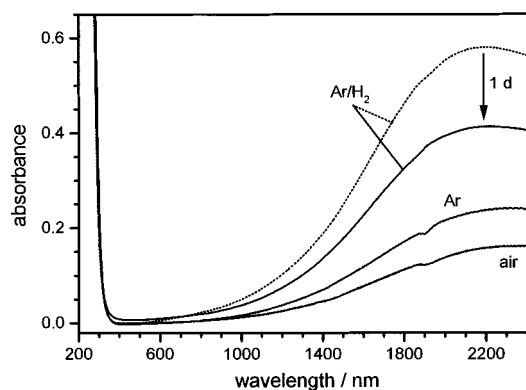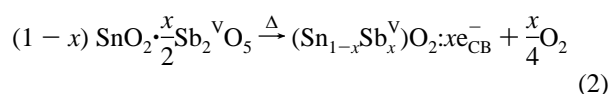
(2)

Figure 5. UV−vis−NIR absorption spectra of SnO_2:Sb colloids prepared using $SbCl_5$ as the source of antimony and autoclaved for 3 h at 270 °C under the indicated atmospheric conditions. The spectra have been acquired in 0.1-mm cuvettes.

Because oxygen must be removed from the lattice, conversion to the n-conductive phase can be expected to proceed faster under a reducing atmosphere or argon. In fact, colloids autoclaved under argon rather than in air for the same period of time, show a more intense coloration and an absorption onset that is located at smaller wavelengths (Figure 5).

The upper two spectra in Figure 5 show that autoclavation under Ar/H_2, i.e., under strongly reducing conditions, increases the absorption intensity further. In accordance with the reaction scheme given above, both spectra show an IR absorption that is more intense and more blue-shifted than the absorption of the same colloid autoclaved under argon or in air. The absorption intensity measured directly after autoclavation (dotted line), however, decreases slightly upon exposure to air until a stable absorption is observed after about 24 h (solid line). Obviously, heating under Ar/H_2 generates additional oxygen vacancies, which, similar to tin dioxide nanoparticles containing no antimony (Figures 1 and 2), are destroyed if the colloid is exposed to air.

In principle, removal of oxygen from the crystal lattice should not be necessary if Sb(V) was replaced by Sb(III) in the synthesis. If we start from a mixed oxide of tin(IV) and antimony(III), i.e., $(1 − x)SnO_2 \cdot (x/2)Sb_2O_3$ in this case, and if we exclude oxygen from the reaction mixture, the reaction scheme should be given by

$$(1 − x)SnO_2 \cdot \frac{x}{2}Sb_2^{III}O_3 \xrightarrow{\Delta} (Sn_{1−x}Sb_x^{V})O_{2−x/2} : 2xe_{CB}^{-}$$

(3)
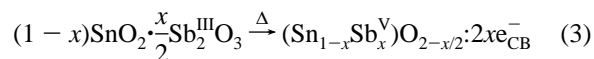
Thus, formation of a heavily n-doped tin dioxide, being both oxygen-deficient and doped with antimony, would be expected. However, a synthesis performed according to reaction scheme 3 would require that oxygen is excluded not only during autoclavation, but also during all other steps, including centrifugation, washing of the precipitate, and dialysis. The reason is that the mixed oxide given on the left-hand side of the reaction scheme is not stable in air. The white precipitate obtained after the hydrochloric solution of $SnCl_4$ and $SbCl_3$ is combined with base develops a yellowish color that turns to brownish during dialysis and refluxing. This color is caused by a strong absorption band close to the band-gap transition[13] and is connected to the simultaneous presence of antimony(III) and antimony(V) in tin dioxide, as shown by near edge X-ray absorption fine structure measurements (XANES) on nanocrystalline powders.[17] The ratio of antimony(III) to antimony-(V) can be determined from the XANES spectra because the position of the Sb L_1 edge is sensitive to the oxidation state of
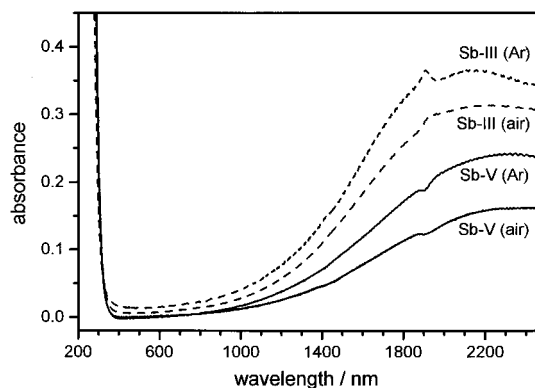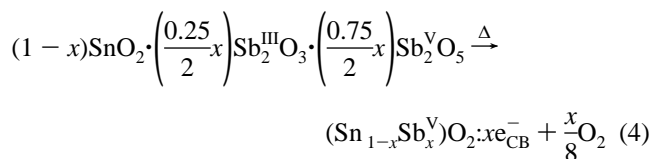
Figure 6. UV−vis−NIR absorption spectra of SnO$_2$:Sb colloids prepared using the indicated antimony precursor and autoclaved for 3 h at 270 °C under the indicated atmospheric conditions. The spectra have been acquired in 0.1-mm-cuvettes.

antimony. For samples obtained by using an antimony(III) precursor, XANES measurements further show that as much as 75% of the Sb^{3+} ions of the starting material are already oxidized to Sb^{5+} at a temperature of 100 °C or lower. In contrast, no change in the oxidation state and no coloration is observed if an Sb(V) compound is used as precursor. The strong tendency of Sb(III) to form Sb(V) in the presence of tin dioxide indicates that incorporation of the small Sb^{5+} ion ($r = 60$ pm) into the tin dioxide lattice (Sn^{4+}, $r = 69$ pm) is energetically more favorable than incorporation of the larger Sb^{3+} ion ($r = 76$ pm).[26]

Autoclavation of the brownish colloid containing Sb(V) and Sb(III) in a ratio of 75:25 yields a bluish product. Assuming that all Sb(III) is converted into Sb(V) during this process, the reaction scheme is given by

$$(1 - x)\text{SnO}_2 \cdot \left(\frac{0.25}{2}x\right)\text{Sb}_2^{\text{III}}\text{O}_3 \cdot \left(\frac{0.75}{2}x\right)\text{Sb}_2^{\text{V}}\text{O}_5 \xrightarrow{\Delta}$$

$$(\text{Sn}_{1-x}\text{Sb}_x^{\text{V}})\text{O}_2{:}x\text{e}_{\text{CB}}^- + \frac{x}{8}\text{O}_2 \quad (4)$$

Compared to reaction scheme 2, only half the amount of oxygen must be removed from the lattice. In fact, colloids autoclaved in air or under argon for a given period of time (Figure 6) show a stronger IR absorption, if Sb(III) instead of Sb(V) is used in the synthesis.

Thus, the results given in Figure 5 and Figure 6 show that the rate of the conversion reaction is influenced by the atmosphere inside the autoclave and by the oxidation state of the antimony source employed.

To determine the degree to which the nonconductive educt is converted into the n-conductive phase, we investigated the intensity of the IR absorption after prolonged autoclavation. Figure 7 displays the absorption spectra of a tin dioxide colloid doped with antimony(V) after heating at 270 °C under argon for different periods of time. The reaction proceeds according to scheme 2. Figure 7 shows that the intensity of the absorption increases with time, and the maximum in the absorption band shifts to shorter wavelength. Attempts to increase the absorption intensity further failed: prolonged heating under argon finally leads to agglomeration. If the reaction is performed under Ar/H$_2$, oxygen vacancies are formed after 3 h of heating (Figure 5). Even longer heating (16 h) under Ar/H$_2$ decreases the intensity of the IR absorption (Figure 8) and turns the blue color of the colloid to greenish-blue. This change in color is caused by an additional absorption band in the blue (inset in Figure 8)
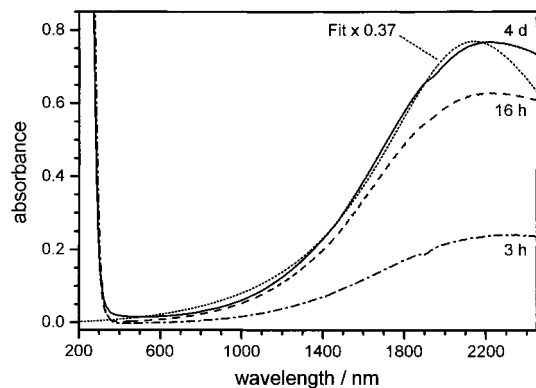

Figure 7. UV−vis−NIR absorption spectra of SnO$_2$:Sb colloids prepared using SbCl$_5$ as the source of antimony and autoclaved under argon for the indicated periods of time at 270 °C. The spectra have been acquired in 0.1-mm cuvettes. Dotted line: Mie−Drude fit to the spectrum of the colloid autoclaved for 4 days.
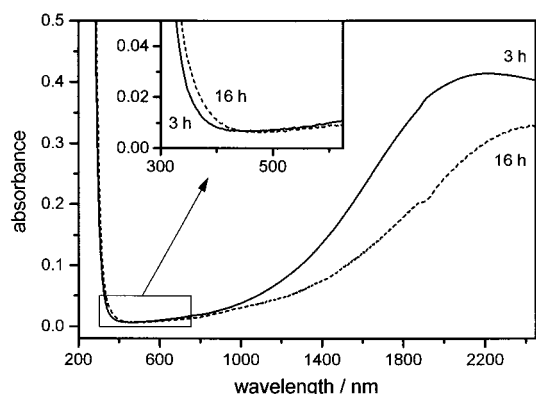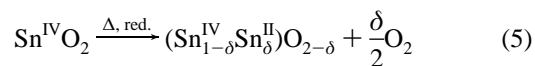

Figure 8. UV−vis−NIR absorption spectra of SnO$_2$:Sb colloids prepared using SbCl$_5$ as the source of antimony and autoclaved under Ar/H$_2$ for the indicated periods of time at 270 °C. The spectra have been acquired in 0.1-mm cuvettes.
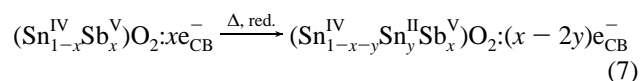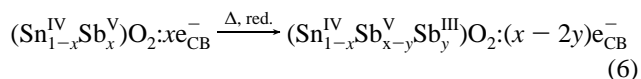
that is likely to be caused by the reduction of Sb^{5+} to Sb^{3+} or by the reduction of Sn^{4+} to Sn^{2+}.

As mentioned above, colloids containing both Sb^{5+} and Sb^{3+} show a strong absorption close to the band-gap transition. Figure 3 shows that an absorption close to the band-gap transition is observed, as well, in colloids of oxygen-deficient tin dioxide containing no antimony. In pure tin dioxide, formation of Sn^{2+} according to

$$\text{Sn}^{\text{IV}}\text{O}_2 \xrightarrow{\Delta, \text{ red.}} (\text{Sn}_{1-\delta}^{\text{IV}}\text{Sn}_\delta^{\text{II}})\text{O}_{2-\delta} + \frac{\delta}{2}\text{O}_2 \qquad (5)$$

competes with the formation of oxygen deficiencies (reaction scheme 1) and seems to be the reason for the weaker IR absorption of oxygen-deficient tin dioxide colloids as compared to antimony doped colloids.

Formation of Sb^{3+} or Sn^{2+} in antimony-doped colloids autoclaved under Ar/H$_2$ may explain the reduced intensity of the IR absorption shown in Figure 8, as these ions are expected to form deep electron traps, reducing the number of free electrons according to

$$(\text{Sn}_{1-x}^{\text{IV}}\text{Sb}_x^{\text{V}})\text{O}_2{:}x\text{e}_{\text{CB}}^- \xrightarrow{\Delta, \text{ red.}} (\text{Sn}_{1-x}^{\text{IV}}\text{Sb}_{x-y}^{\text{V}}\text{Sb}_y^{\text{III}})\text{O}_2{:}(x - 2y)\text{e}_{\text{CB}}^-$$
$$(6)$$

$$(\text{Sn}_{1-x}^{\text{IV}}\text{Sb}_x^{\text{V}})\text{O}_2{:}x\text{e}_{\text{CB}}^- \xrightarrow{\Delta, \text{ red.}} (\text{Sn}_{1-x-y}^{\text{IV}}\text{Sn}_y^{\text{II}}\text{Sb}_x^{\text{V}})\text{O}_2{:}(x - 2y)\text{e}_{\text{CB}}^-$$
$$(7)$$

Thus, the results given above show that application of strongly reducing conditions causes several side reactions to occur but does not lead to a further increase of the IR absorption. In the following, we compare the maximum intensity of the IR absorption in Figure 7 with the expected intensity as calculated from Mie theory.

According to Mie theory, the absorbance of the plasmon polariton band is given by[10]

$$A = -\log\left(\frac{I}{I_0}\right) = \frac{18\pi}{\ln(10)} \frac{10^4 M \epsilon_{\mathrm{m}}^{3/2}}{\lambda} \frac{\epsilon'}{\rho} \frac{\epsilon'}{(\epsilon' + 2\epsilon_{\mathrm{m}})^2 + \epsilon''^2} Cd \quad \text{(I)}$$

where λ is the wavelength of the incident light, d is the thickness of the cuvette, and ϵ_{m} is the dielectric constant of the embedding medium, i.e., water. The molecular weight of tin dioxide, its density, and its concentration in moles per liter of colloid are given by M, ρ, and C, respectively. The real and imaginary parts of the dielectric function of tin dioxide correspond to ϵ' and ϵ'', respectively. For bulk tin dioxide containing amounts of antimony similar to those in our nanoparticles, the complex dielectric function $\epsilon = \epsilon' + i\epsilon''$ has been shown to be very well described by the Drude theory.[4] Hence, ϵ' and ϵ'' are given by

$$\epsilon' = \epsilon_\infty - \frac{\omega_N^2}{\omega^2 + \Gamma^2} \quad \text{(II)}$$

and

$$\epsilon'' = \frac{\omega_N^2 \Gamma}{\omega(\omega^2 + \Gamma^2)} \quad \text{(III)}$$

Here, ϵ_∞ is the high-frequency dielectric constant of tin dioxide. The angular frequency ω is related to the wavelength of incident light by $\omega = 2\pi c/\lambda$, and Γ is the number of scattering events per second for the electrons. The frequency ω_N is related to the number density of conduction-band electrons N_e and their effective mass m_{eff} by $\omega_N^2 = N_e e^2/(m_{\mathrm{eff}}\epsilon_0)$. Hence, ω_N^2 is determined by the ratio N_e/m_{eff}. Throughout this paper, we use a value of $m_{\mathrm{eff}} = 0.33m_0$, which has been deduced from Hall measurements on dense SnO$_2$:Sb films doped with 3 atom % of antimony.[27]

By using the expressions above and values of $N_e = 6.0 \times 10^{20}$ cm^{-3}, $\Gamma = 5.06 \times 10^{14}$ s^{-1}, and $\epsilon_{\mathrm{m}} = 1.77$, the spectral position and the onset of the IR absorption of the nanoparticles are well reproduced (dotted line in Figure 7). The carrier concentration is in agreement with the maximum value obtained by Hall measurements of SnO$_2$:Sb layers doped with 4 atom % antimony.[28]

The scattering parameter Γ is related to the velocity v_{F} of electrons at Fermi energy and their mean free path L by $\Gamma = v_{\mathrm{F}}/L$. For spherical nanoparticles, the mean free path of conduction-band electrons is given by $1/L = 1/R + 1/L_{\mathrm{bulk}}$,[29] where R is the radius of the nanoparticle and L_{bulk} is the mean free path of carriers in bulk material. Using values of $R = 2.5$ nm, which is in accordance with the XRD data, and $v_{\mathrm{F}} = 10^6$ m/s (i.e., a value typical for metals[30]), the scattering parameter Γ obtained above corresponds to values of $L = 2.0$ nm and $L_{\mathrm{bulk}} = 10$ nm for the mean free path of electrons in the nanoparticles and bulk material, respectively.

However, Figure 7 also shows that the intensity of the absorption is about three times weaker than calculated. Moreover, the absorption at higher wavelengths is broader than expected. Both deviations indicate that the electron density is not homogeneous throughout the sample volume. Two limiting cases of spatial inhomogeneity can be considered.

In the first model, the sample is assumed to consist of nanoparticles with different number densities of free electrons, whereas the electron density inside each particle is constant throughout the particle volume. Conductivity measurements and Hall measurements of layers of highly doped SnO$_2$:Sb[1,28,31] show that the carrier density is restricted to about 8×10^{20} cm^{-3}. If the electron density is close to this value, then an increase in the concentration of antimony will not lead to an increased concentration of carriers. The electron density in our samples is close to this limiting value. Therefore, if the antimony content of the nanoparticles varies, the concentration of antimony in some particles will be so high that only a fraction of antimony leads to the formation of conduction-band electrons. Because these particles contain more antimony than the average value of 6 atom %, the distribution also must contain particles with low antimony content and, hence, low electron densities. As a consequence, the absorption peak of the sample will be broader and its peak intensity somewhat lower than expected (eq I). Furthermore, the broadening of the peak will be pronounced at its low-energy side, which corresponds to particles with low electron densities.

In the second model, all particles are assumed to have about the same overall electron density, but the carrier concentration in each particle varies over the particle volume. Very often, grains of SnO$_2$:Sb are thought to be composed of a core with high electron density and a surface layer exhibiting a much lower electron density. An electrically isolating or weakly conducting surface layer may explain the strong grain boundary resistance[13,14,32] often observed in layers of this material.

A surface layer with low electron density is expected if the surface region of the particles is enriched, for instance, with Sb(III) or with interstitial oxygen atoms acting as electron traps. In fact, surface enrichment by antimony has been frequently observed in SnO$_2$:Sb prepared at high temperatures.[33−35] Mössbauer measurements[36] on samples containing both Sb(III) and Sb(V) indicate that the Sb^{3+} ions are located at surface or grain boundary sites, whereas Sb(V) is located mainly in the particle core. Moreover, incorporation of oxygen into the surface of SnO$_2$:Sb is known to reduce the electrical conductivity of the material, enabling the use of SnO$_2$:Sb layers as gas sensors.[37]

Even in the absence of electron trapping, the surface layer of the nanoparticles should be partly depleted of electrons, as highly n-doped nanoparticles in aqueous solution are expected to form a space-charge layer at the particle surface. This was noted recently by Boschloo and Fitzmaurice,[15] who investigated the electrochemical properties of nanostructured electrodes consisting of a porous network of highly n-doped SnO$_2$:Sb nanoparticles. Under open-circuit conditions, this space-charge layer is depleted of electrons, as indicated in Figure 9.

The thickness Δr of the depletion layer is related to the number density N_D of ionized donors in the particle core (and, hence, to the electron density) and to the potential drop ϕ_{SC} at the particle surface by[15,38,39]

$$\phi_{\mathrm{SC}}(\Delta r) = \frac{e N_D}{6\epsilon\epsilon_0}\left(3 - 2\frac{\Delta r}{R}\right)\Delta r^2 \quad \text{(IV)}$$

where R is the radius of the particles, e is the elementary charge, ϵ is the static dielectric constant of the semiconductor, and ϵ_0 is the dielectric constant of vacuum. Boschloo and Fitzmaurice varied the potential drop ϕ_{SC} at the particle surface and, hence, the thickness of the depletion layer by applying an external
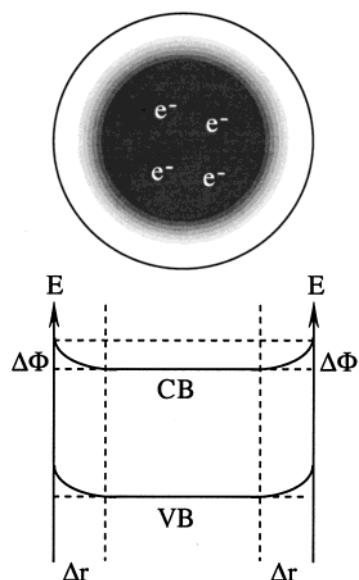
Figure 9. Upper part: Distribution of conduction-band electron densities in a highly n-doped semiconductor nanoparticle. Lower part: Potential drop Φ_{SC} across the space-charge layer, depletion layer with thickness Δr, and band bending of the nanoparticle.

voltage to their nanoporous electrode. At negative potentials, electrons were injected into the nanoparticles, accompanied by a decrease of the potential drop ϕ_{SC} and, hence, a decrease of the thickness of the space-charge layer. Because of the injection of electrons, the blue color of the electrodes was intensified. A similar change in color is observed in our colloidal solutions if electrons are injected into the colloidal nanoparticles via an optically transparent thin film electrode.[13]

If we assume the surface layer to be totally depleted of electrons, a spherical particle with a diameter of $2R = 50$ Å will have to consist of a core with a diameter of 36 Å and a depletion layer with a thickness of about 7 Å in order to explain the difference between the experimentally observed IR absorption spectrum and Mie theory. In this case, the volume fraction containing free electrons is given by $V_{core}/V_{total} = 0.37$, i.e., a value equal to the factor by which the observed IR intensity is lower than predicted (see Figure 7).

If we completely neglect trapping of electrons at the particle surface, the potential drop ϕ_{SC} corresponding to $\Delta r = 7$ Å can be calculated from eq IV. Using a density of ionized donors of $N_D = 6.0 \times 10^{20}$ cm^{-3}, a static dielectric constant of $\epsilon = 10$, and values for R and Δr as given above, a potential drop of $\phi_{Sc} = 0.22$ V is calculated, which is within the expected range of about $0.1-1$ V.

Therefore, it seems likely that the low intensity of the IR absorption is mainly caused by an insulating surface layer around each particle and, to a lesser extent, by inhomogeneous doping. This picture is in accord with electrochemical and impedance measurements of SnO$_2$:Sb nanoparticle layers, which will be presented in a forthcoming paper.[16]

Summary

Colloidal solutions of rutile-type SnO$_2$ nanoparticles with particle diameters ranging from 4 to 9 nm have been prepared in an autoclave at elevated temperatures. Particles doped with antimony or containing oxygen deficiencies display a strong absorption band in the red and IR regions. The IR absorption band of the nanoparticles consists of a broad peak rather than a steplike absorption onset observed in the bulk material. Antimony(III) sources as well as antimony(V) sources can be used to prepare stable n-doped SnO$_2$:Sb nanoparticles. In contrast, oxygen vacancies in oxygen-deficient nanoparticles are not stable in air. Reaction schemes have been provided to explain the formation of n-doped particles under the various reaction conditions applied.

Even after prolonged heating, the intensity of the IR absorption in antimony-doped nanoparticles is found to be about three times weaker than expected from Mie theory. This deviation is explained by a layer at the surface of the nanoparticles that is depleted of electrons.

References and Notes

(1) Chopra, K. L.; Major, S.; Pandya, D. K. *Thin Solid Films* **1983**, *102*, 1.

(2) Herrmann, J.-M. J.; Portefaix, J.-L.; Forissier, M.; Figueras, F.; Pichat, P. *J. Chem. Soc., Faraday Trans.* **1979**, *1*, 1346.

(3) Koch, H. *Phys. Status Solidi* **1963**, *3*, 1059.

(4) Shanthi, E.; Dutta, V.; Banerjee, A.; Chopra, K. L. *J. Appl. Phys.* **1980**, *51*, 6243.

(5) Mishra, K. C.; Johnson, K. H. *Phys. Rev. B* **1995**, *51* (20), 13972.

(6) Frank, G.; Kauer, E.; Köstlin, H. *Thin Solid Films* **1981**, *77*, 107.

(7) Hamberg, I.; Granqvist, C. G. *J. Appl. Phys.* **1986**, *60*, R123.

(8) Grosse, P. *Freie Elektronen in Festkörpern*; Springer-Verlag: Berlin, Germany, 1979.

(9) Kittel, Ch. *Introduction to Solid State Physics*, 6th ed.; John Wiley & Sons: New York, 1986.

(10) Henglein, A. *J. Phys. Chem.* **1993**, *97*, 5457.

(11) Link, S.; El-Sayed, M. A. *J. Phys. Chem. B* **1999**, *103*, 8410

(12) Dawar, A. L.; Joshi, J. C. *J. Mater. Sci.* **1984**, *19*, 1.

(13) Nütz, T.; zum Felde, U.; Haase, M. *J. Chem. Phys.* **1999**, *110* (24), 12142.

(14) van Bommel, M. J.; Groen, W. a.; van Hal, H. A. M.; Keur, W. C.; Bernards, T. N. M. *J. Mater. Sci.* **1999**, *34*, 4803.

(15) Boschloo, G.; Fitzmaurice, D. *J. Phys. Chem. B* **1999**, *103*, 3093.

(16) zum Felde, U.; Haase, M.; Weller, H. *J. Phys. Chem.*, accepted.

(17) Rockenberger, J.; zum Felde, U.; Tischer, M.; Tröger, L.; Haase, M.; Weller, H. *J. Chem. Phys.* **2000**, *112*, 4296.

(18) Vincent, C. A.; Weston, D. G. C. *J. Electrochem. Soc.* **1972**, *119* (4), 519.

(19) Crnjak-Orel, Z.; Orel, B.; Hodoscek, M.; Kaucic, V. *J. Mater. Sci.* **1992**, *27*, 313.

(20) Orel, B.; Lavrencic-Stangar, U.; Crnjak-Orel, Z.; Bukovec, P.; Kosec, M. *J. Non-Cryst. Solids* **1994**, *167*, 272.

(21) Jarzebski, Z. M.; Marton, J. P. *J. Electrochem. Soc.* **1976**, *123* (9), 299C.

(22) Marley, J. A.; Dockerty, R. C. *Phys. Rev. A* **1965**, *140*, 304.

(23) Fonstad, C. G.; Rediker, R. H. *J. Appl. Phys.* **1971**, *42*, 2911.

(24) Samson, S.; Fonstad, C. G. *J. Appl. Phys.* **1973**, *44* (10), 4618.

(25) Sanjinés, R.; Demarne, V.; Lévy, F. *Thin Sold Films* **1990**, *193/194*, 935.

(26) Shannon, R. D. *Acta Crystallogr.* **1976**, *A32*, 751.

(27) Shanthi, E.; Banerjee, A.; Dutta, V.; Chopra, K. L. *J. Appl. Phys.* **1982**, *53* (3), 1615.

(28) Terrier, C.; Chatelon, J. P.; Roger, J. A. *Thin Solid Films* **1997**, *295*, 95.

(29) Mulvaney, P. *Langmuir* **1996**, *12* (3), 788.

(30) Kittel, C. *Introduction to Solid State Physics*, 6th ed.; John Wiley & Sons: New York, 1986.

(31) Kaneko, H.; Miyake, K. *J. Appl. Phys.* **1982**, *53* (5), 3629.

(32) Orel, B.; Lavrencic Stangar, U.; Opara, U.; Gaberscek, M.; Kalcher, K. *J. Mater. Chem.* **1995**, *5* (4), 617.

(33) Cross, Y. M.; Pyke, D. R. *J. Catal.* **1979**, *58*, 61.

(34) Cox, P. A.; Egdell, R. G.; Harding, C.; Patterson, W. R.; Tavener, P. J. *Surf. Sci.* **1982**, *123*, 179.

(35) Egdell, R. G.; Flavell, W. R.; Tavener, P. *J. Solid State Chem.* **1984**, *51*, 345.

Wet-Chemical Synthesis of Doped Nanoparticles

J. Phys. Chem. B, Vol. 104, No. 35, 2000 **8437**

(36) Berry, F. J.; Laundy, B. J. *J. Chem. Soc.*, *Dalton Trans.* **1981**, 1442.

(37) Dusastre, V. D. Williams, E. *J. Phys. Chem. B* **1998**, *102*, 6732.

(38) Albery, W. J.; Bartlett, P. N. *J. Electrochem. Soc.* **1984**, *131* (2), 315.

(39) Goossens, A. *J. Electrochem. Soc.* **1996**, *143* (6), L131.